



Blended polar/nonpolar peptide conjugate interferes with human insulin amyloid-mediated cytotoxicity

Shantanu Sen^a, Prerana Singh^b, Narendra Kumar Mishra^{a,1}, Subramaniam Ganesh^{b,*},
Sri Sivakumar^{c,d,e,f,*}, Sandeep Verma^{a,d,e,*}

^a Department of Chemistry, Indian Institute of Technology Kanpur, Kanpur 208016, UP, India

^b Department of Biological Sciences & Bioengineering, Indian Institute of Technology Kanpur, Kanpur 208016, UP, India

^c Department of Chemical Engineering, Indian Institute of Technology Kanpur, Kanpur 208016, UP, India

^d Centre for Nanoscience, Indian Institute of Technology Kanpur, Kanpur 208016, UP, India

^e Centre for Environmental Science & Engineering, Indian Institute of Technology Kanpur, Kanpur 208016, UP, India

^f Material Science Programme, Indian Institute of Technology Kanpur, Kanpur 208016, UP, India

ARTICLE INFO

Keywords:

Insulin
Aggregation
Inhibition
Peptide inhibitor
Palmitoylated-peptide conjugate
Hydrophobicity
Amyloid-mediated cytotoxicity
Cytoprotective

ABSTRACT

Insulin, a peptide hormone and a key regulator of blood glucose level, is routinely administered to type-I diabetic patients to achieve the required glycemic control. Insulin aggregation and ensuing amyloidosis has been observed at repeated insulin injection sites and in injectable formulations. The latter occurs due to insulin agglomeration during shipping and storage. Such insulin amyloid leads to enhanced immunogenicity and allow potential attachment to cell membranes leading to cell permeability and apoptosis. Small molecule inhibitors provide useful interruption of this process and inhibit protein misfolding as well as amyloid formation. In this context, we report the propensity of a palmitoylated peptide conjugate to inhibit insulin aggregation and amyloid-mediated cytotoxicity, via designed interference with polypeptide interfacial interactions.

1. Introduction

Protein aggregation and amyloidosis is a major physical transformation leading to debilitating pathophysiological conditions with far-reaching clinical consequences. Till now, many diseases such as Huntington's disease, Alzheimer's disease, Parkinson's disease, Prion-associated encephalopathies, to name a few, are known to be associated with protein aggregation [1]. Agglomeration in therapeutic polypeptides and proteins can also interfere with their (bio)processing during shipping and storage. Latter necessitates deeper understanding of the process for therapeutic proteins/polypeptides and its ramifications due to adverse responses in patients. Immunogenic nature of such aggregated therapeutic proteins could curtail synthesis processes, product development and present undesired health risk issues.

Pharmaceutical insulin formulations availed for diabetic patients also encounter similar problems for its aggregating tendency and known to initiate formation of lobules due to increase in aggregate accumulation at repeated insulin injection sites causing 'injection-localized

amyloidosis' [2,3]. Aggregates present in insulin injectable may also lead to enhanced immunogenicity in patients [4]. With time insulin aggregation leads to its shorter shelf-life, reduced bioavailability and undesired deposition. Different factors of the exposed environment such as pH, ionic strength of the environment, agitation, temperature, storage conditions, properties of contact surfaces etc. may destabilize insulin and further promote its aggregation. Hence, the ability to modulate or inhibit aggregation is not only important for therapeutic reasons, but is also needed to safeguard storage and suppress adventitious side-reactions.

Misfolded protein monomers aggregate due to synergistic cooperation from intermolecular forces including hydrophobic and aromatic-aromatic interactions, causing loss of native three-dimensional structure leading to thermodynamically stable amyloidogenic protein ensembles with the ability to trigger cytotoxicity [5,6]. In many instances, protein aggregates have been reported for cellular damage via initiation of apoptotic events. Although, definite mechanisms involved in toxic amyloid triggered cellular apoptosis yet to be explored further.

* Corresponding authors at: Department of Chemistry, Indian Institute of Technology Kanpur, Kanpur 208016, UP, India (S. Verma). Department of Chemical Engineering, Indian Institute of Technology Kanpur, Kanpur 208016, UP, India (S. Sivakumar).

E-mail addresses: sganesh@iitk.ac.in (S. Ganesh), srisiva@iitk.ac.in (S. Sivakumar), sverma@iitk.ac.in (S. Verma).

¹ Current address: Department of Chemistry, University of Copenhagen, Universitetsparken 5, DK-2100 Copenhagen Ø, Denmark.

However, apoptotic events are cumulatively contributed by protein aggregate mediated inflammatory responses, destabilization as well as permeabilization of cellular membrane. Elevated cellular stress through reactive oxygen species overproduction, cytokine overproduction and activation of caspases etc were correlated as some of the resultant apoptotic events [7]. Apoptotic cells can be distinguished from their nuclear fading caused due to dissolution of chromatin by DNase and RNase, nuclear shrinkage due to chromatin condensation, rupturing of nuclear membrane and nuclear DNA fragmentation [8]. Insulin amyloid-mediated cell apoptosis has already been reported in many instances [9–11].

Previous studies have shown significant implications of design strategies in formulating such peptide-based inhibitors composed of aromatic amino acid residues, having significant inhibitory efficacy of protein aggregation [12–15]. Further approaches including hybrid peptides, bio-inspired peptides, aromatic compounds, nanoparticles, metal complexes, trehalose, polycyclic compounds etc. have also been demonstrated for delaying or inhibiting insulin aggregation process [16–21].

Cytotoxic nature of insulin fibril was linked up to their detergent like capability of disaggregating cellular membranes in contact. Exposed hydrophobic patches of misfolded inactive insulin monomers are known to be involved in generation of insoluble toxic fibrillar aggregates [22–24]. Hence, hydrophobic character driven engagement of such patches would curtail or inhibit the aggregation process. Sufficient evidences of hydrophobicity mediated fibrillation inhibition phenomena encourage us to probe the inhibitory efficacy of the inspired newly designed construct **1** (Fig. 1) [25].

Compound **1** is constructed from the hydrophobic chain of palmitic acid conjugated at *N*-terminal, polar taurine residue at C-terminal and sandwiched aromatic tryptophan residues (Trp-Trp). We have reported on the potential of Trp-Trp-Taurine sequence interacting with the aromatic tripeptide stretch of Phe²⁴Phe²⁵Tyr²⁶, C-terminal hydrophobic sequence of insulin B chain important for its native dimerization, in modulating hydrophobic interactions between insulin molecules and preventing their fibrillation [12,13]. We anticipated that the introduction of a palmitoyl chain would provide additional hydrophobic character enabling the new construct to further interact with exposed hydrophobic residues of monomeric insulin, under applied stress conditions for self-aggregation.

This whole conjugate itself making micelle kind of structures in solution phase due to its amphiphilic built. Critical micelle concentration (CMC) of compound **1** was estimated to be ~10 μ M (Fig. S9). Whereas, no such micelle formation was observed for Trp-Trp-Tau alone at corresponding concentrations (Fig. S10). Apart from providing hydrophobicity, palmitic acid is also highly biocompatible in terms of its utilization as a part of any drug candidate. As palmitic acid is highly abundant in our body and found in approximately 5% of our total body weight [26]. Some of the existing excipients were also employed in combination with palmitic acid in several formulations used for drug

delivery. Besides, Trp-Trp conjugation is also vital as it provides π - π interactions in addition to terminal polarity of taurine residue as well as non-polarity of palmitic acid. We hypothesized that precisely orchestrated amphiphilic character of **1** will induce self-assembled nanostructures. Indeed, merged polarity and non-polarity of such nanostructures will result in insulin aggregation inhibition by altering the pathways for amyloidosis as well as solubilizing any traceable toxic insulin aggregates and thus hinder harmful interactions of aggregates with critical cellular components [27,28]. Similar advantage of blended polarity/non-polarity was reported for a surfactant (a myristoylated phenylalanine conjugate with a polyether hydrophilic group) stabilizing model protein drugs during heat-aging aggregation [15]. The following study has been carried out to demonstrate the favourable outcome regarding improved inhibitory efficacy after adapting the above mentioned strategy.

2. Materials and methods

2.1. General information

Human insulin (HI), FITC-phalloidin, trypsin - ethylenediaminetetraacetic acid (trypsin-EDTA), Dulbecco's modified eagle medium (DMEM), Triton X-100, 3-(4,5-dimethylthiazol-2-yl)-2,5-diphenyltetrazolium bromide (MTT) were purchased from Sigma Aldrich and Thioflavin T from Fluka. Penicillin-streptomycin antibiotic solution was purchased from HiMedia. Dimethyl sulfoxide (DMSO) was obtained from Merck Chemicals, India. Foetal Bovine Serum (FBS) was purchased from Gibco Life Technologies. HeLa (Carcinoma) cells were procured from National Centre for Cell Science (NCCS), Pune. DAPI and Hoechst were purchased from Thermo fisher. Acridine Orange (AO) and Ethidium bromide (EtBr) were procured from Sigma Aldrich. The chemicals used for *in vitro* cell culture experiments were used as received. All solvents used for these experiments were distilled prior to use following standard procedures. All chemicals and resins were purchased from Spectrochem, Mumbai, India and used without further purification. ¹H NMR spectra were recorded on JEOL-ECS 400 model operating at 400 MHz and ¹³C NMR spectra were recorded on JEOL-DELTA2 500 model operating at 500 MHz. High resolution mass spectra (HRMS) were recorded at IIT Kanpur, India, on Waters, Q-ToF Premier micromass HAB 213 mass spectrometer using a capillary voltage of 2.6–3.2 kV.

2.2. Synthesis of Palmitoylated Trp-Trp-Tau peptide (**1**)

Palmitoylated Trp-Trp-Tau was synthesized and characterized as shown in the supporting information (Scheme S1). ¹H NMR spectra, ¹³C NMR spectra and HRMS-ESI data for the final synthesized compound were also provided (Figure S12-S14).

2.3. Thioflavin T (ThT) binding assay

Freshly prepared insulin and insulin mixed with different peptide conjugates, were incubated at 65 °C in 0.1 N HCl water (pH 1.6) with an additional salt concentration of 25 mM NaCl. ThT dye was added to reaction volume to attain a final concentration of 20 μ M. Fluorescence intensity was measured at room temperature with an excitation wavelength (λ_{ex}) of 410 nm and observed emission wavelength (λ_{em}) at 488 nm. The aggregation behavior of insulin alone and in presence of the peptide conjugates were studied for the insulin concentration of 0.5 mg/mL (~86 μ M). Fluorescence spectra were recorded with a 10 mm quartz cells at 65 \pm 0.1 °C using a Varian Luminescence Cary Eclipse. Three consecutive scans were taken for each sample and the average spectra was plotted by Origin 9.1 software (Fig. 2). All the observations were carried out under a fixed bandpass of 5 nm in addition to a magnetic stirrer maintaining sample homogeneity at 800 rpm. AR-grade hydrochloric acid and HPLC-grade water were used for every preparation

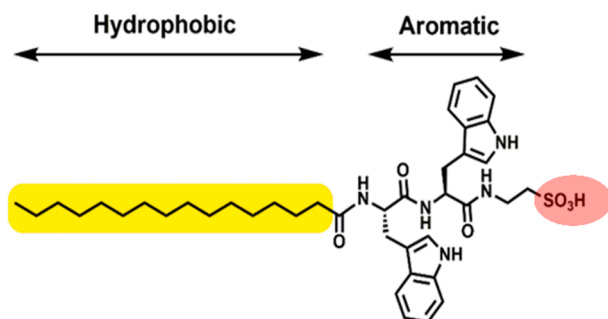


Fig. 1. Palmitoylated Trp-Trp-Tau peptide (**1**): blended polar and nonpolar patches.

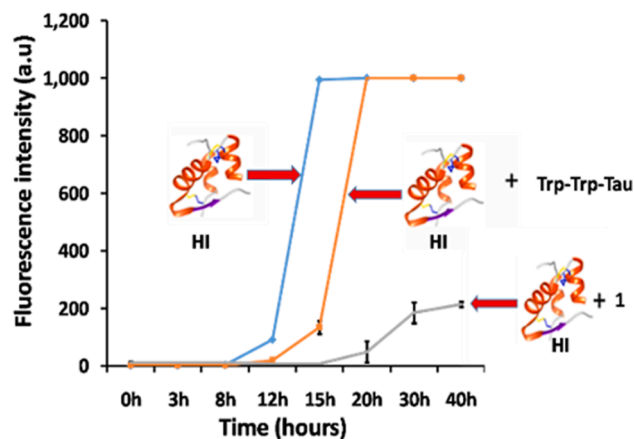


Fig. 2. Thioflavin T fluorescence spectra of human insulin ($\sim 86 \mu\text{M}$) aggregation as well as its inhibition by Trp-Trp-Tau ($100 \mu\text{M}$) and compound 1 ($100 \mu\text{M}$).

involved in this study.

2.4. Circular dichroism (CD) spectroscopy

Freshly prepared solution of insulin ($\sim 86 \mu\text{M}$) was either incubated alone or with 1 ($100 \mu\text{M}$) at 65°C in water (pH 1.6) with 25 mM NaCl. All experiments were carried out at room temperature. Spectra were collected for a diluted incubated samples of insulin ($17 \mu\text{M}$) procured at different time points from the incubated reaction mixture, using JASCO J-815 CD spectrometer and a quartz cuvette of 1 mm path length. CD spectra were collected between 195 and 300 nm and each spectrum represents the average of three scans (Fig. 3). To avoid any instrumental baseline drift contributed by the working solution, the background values were subtracted from each individual sample measurement.

2.5. Fourier transform infrared (FTIR) spectroscopy

ATR-FTIR spectra were recorded with a PerkinElmer Spectrum Two Fourier transform spectrometer equipped with peltier stabilized detector. To avoid any instrumental baseline drift contributed by the working solution (water of pH 1.6 with 25 mM NaCl), the background value was subtracted for each individual sample measurement. All experiments were carried out at room temperature, and spectra were collected after

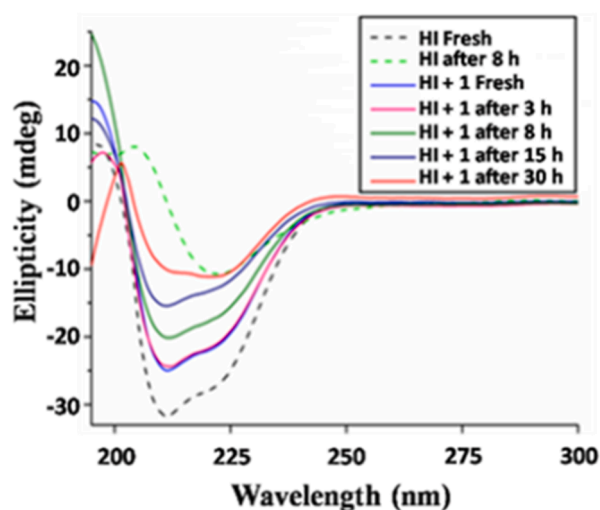


Fig. 3. Far UV-CD spectra during human insulin ($\sim 86 \mu\text{M}$) aggregation and its interference by compound 1 ($100 \mu\text{M}$).

five folds dilution ($17 \mu\text{M}$) of incubated samples of insulin, procured at different time intervals in the absence and presence of compound 1 ($100 \mu\text{M}$) (Fig. 4).

2.6. Native Gel-electrophoresis

Native (non-denaturing) polyacrylamide gel electrophoresis was performed at a constant voltage at 30 mA with a Bio-Rad mini-PROTEIN II electrophoresis system using 15% Tris-HCl polyacrylamide gel. Aliquots of equal volumes of human insulin samples ($\sim 86 \mu\text{M}$) were collected at different time intervals incubated in absence and presence of 1 ($100 \mu\text{M}$) and directly loaded to the gel without any processing. The gels were stained with coomassie blue stain and further destained overnight (Fig. 5).

2.7. Atomic force microscopy (AFM)

Freshly prepared and aged incubated samples of insulin ($\sim 86 \mu\text{M}$) alone and mixed with compound 1 ($100 \mu\text{M}$) were imaged with an atomic force microscope (Molecular Imaging, USA). The machine was operating under the Acoustic AC mode (AAC) with 0.6 N/m force constant and 150 kHz of resonant frequency, with the aid of a cantilever [NSC 12(c) from MikroMasch]. A portion of $10 \mu\text{L}$ of fresh and incubated samples was diluted by $90 \mu\text{L}$ of solution containing water (pH 1.6) and 25 mM NaCl. $5 \mu\text{L}$ of sample from the final cocktail was deposited uniformly using a spin coater operating at speed of 200–500 rpm (PRS-4000), onto a freshly cleaved glass surface at room temperature. The sample-coated glass was dried at room temperature for overnight duration without any contact of dust particles and followed by AFM imaging. Final images of the AFM micrographs were acquired by Pico scan 5 software and extensive analysis of data was done by using visual SPM (Fig. 6).

2.8. MTT assay

MTT (3-(4,5-Dimethylthiazol-2-yl)-2,5-Diphenyltetrazolium Bromide) reduction assay was used to analyze the biocompatibility of compound 1 by determining the cytotoxicity of HeLa cells treated with it. Varying concentrations of compound 1 were added to different sets of cultured HeLa cells in 96-well plate. A set of untreated HeLa cells was used as control. Only viable cells are capable of reducing MTT into blue formazan crystals. Hence, reduction in formazan crystals can directly be correlated with the reduction in cellular viability due to compound's cytotoxicity. Initially cells were seeded at 5000 cells/well in a 96 well plate and incubated for 7 h for cells to adhere before the compound treatment. Stock solution of 1 was prepared by diluting in DMEM cell culture media and added to cells to attain final compound 1 concentrations of 50, 100 and $200 \mu\text{M}$, following incubation for 24 h [37°C , humidified atmosphere with 5% CO_2]. Further, MTT solution in serum free media (0.5 mg/ml) was added to the wells and incubated for 4 h in the CO_2 incubator. After carefully removing the supernatant, $200 \mu\text{L}$ of DMSO was added and incubated for 20 min to dissolve the formazan crystals. The absorbance at 570 nm was analysed using Thermo Scientific Multiskan Spectrum (UV – vis spectrometer) and percentage of cell viability was measured (Fig. 7).

2.9. Hoechst 33342 staining

Hoechst 33342 (Invitrogen, H3570) staining was carried out for detection of apoptotic cells. HeLa cells were grown on gelatin coated coverslips in 24 well plates at a cellular density of 5×10^4 per well and incubated at 37°C in a humidified atmosphere with 5% CO_2 . Compound 1 ($100 \mu\text{M}$) treated or untreated, 48 h aged insulin samples ($\sim 86 \mu\text{M}$) in PBS (pH 7.4) were mixed with HeLa cells to attain final protein concentration of $40 \mu\text{M}$. A set of untreated HeLa cells as control were also cultured which were devoid of any exposure to insulin. After 24 h of

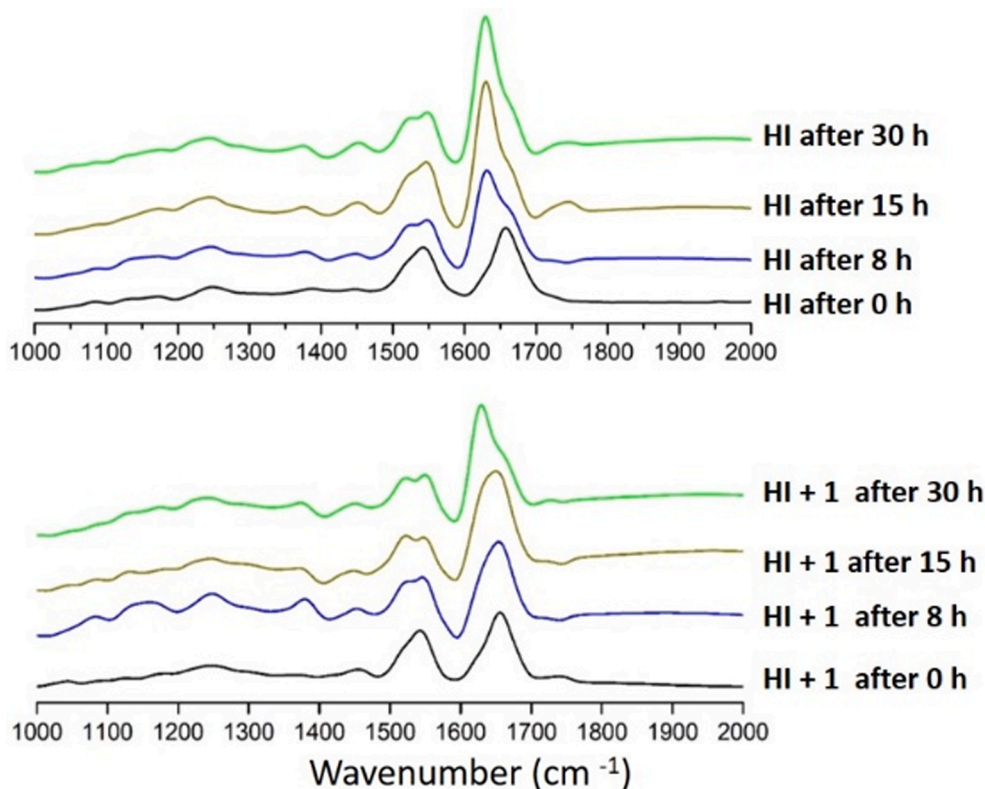


Fig. 4. Time dependent ATR – FTIR spectra of HI ($\sim 86 \mu\text{M}$) aggregation and its interference by compound **1** ($100 \mu\text{M}$).

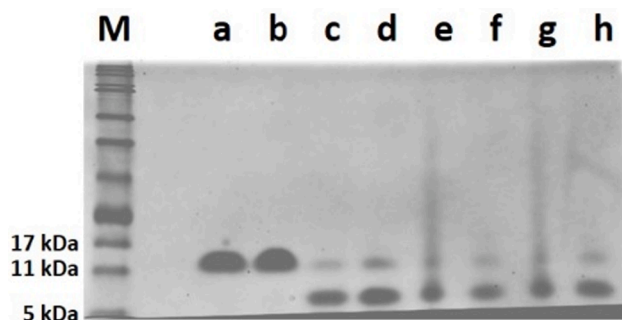


Fig. 5. Native polyacrylamide gel-electrophoresis of (M) Protein molecular weight marker; (a) 0 h aged HI ($\sim 86 \mu\text{M}$); (b) 0 h aged HI ($\sim 86 \mu\text{M}$) co-incubated with **1** ($100 \mu\text{M}$); (c) 3 h aged HI ($\sim 86 \mu\text{M}$); (d) 3 h aged HI ($\sim 86 \mu\text{M}$) co-incubated with **1** ($100 \mu\text{M}$); (e) 8 h aged HI ($\sim 86 \mu\text{M}$); (f) 8 h aged HI ($\sim 86 \mu\text{M}$) co-incubated with **1** ($100 \mu\text{M}$); (g) 30 h aged HI ($\sim 86 \mu\text{M}$); (h) 30 h aged HI ($\sim 86 \mu\text{M}$) co-incubated with **1** ($100 \mu\text{M}$).

incubation, the cells were washed with PBS, fixed with 4%

formaldehyde and stained with Hoechst 33342 dye ($1 \mu\text{g}/\text{mL}$) for 20 min at room temperature. Finally, the cells were washed with PBS thrice to ensure complete removal of unbound stain. The samples were then mounted and images were visualized using confocal microscope (Figs. 8 & S7).

2.10. Cytotoxicity and cellular integrity

HeLa cells were stained with FITC-phalloidin and DAPI to detect any significant changes in cytoskeletal and nuclear morphology respectively. Insulin ($\sim 86 \mu\text{M}$) with or without compound **1** ($100 \mu\text{M}$) were first incubated at 65°C in PBS buffer (pH 7.4) for 48 hrs. HeLa cells were grown on gelatin coated coverslips in 24 well plates at a cellular density of 5×10^4 cells/well and incubated at 37°C in a humidified atmosphere with 5% CO_2 . Compound **1** treated or untreated insulin samples in PBS buffer were directly added to attain a final concentration of $40 \mu\text{M}$. A set of untreated HeLa cells was used as negative control. The cells were treated with the compounds for 24 h followed by fixation with 4% formaldehyde solution for 20 min. Further, the cells were washed with PBS and permeabilized with 0.1% Triton-X 100 for 10 min. The cells

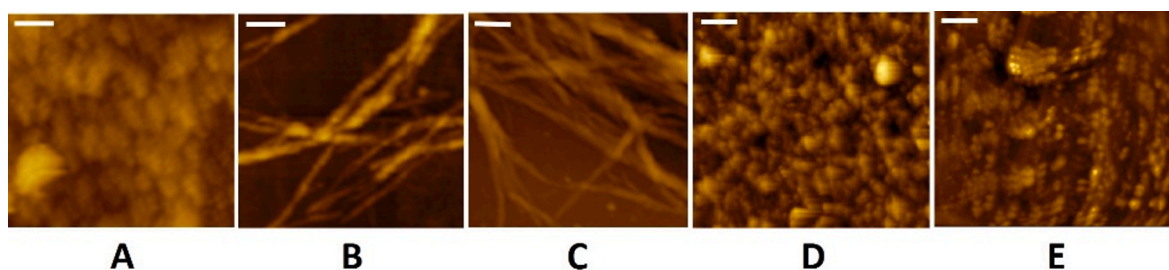


Fig. 6. Time-dependent AFM micrographs (scale bar – 200 nm) of HI ($\sim 86 \mu\text{M}$) incubated for (A) 0 h, (B) 10 h and (C) 30 h. AFM micrographs of HI ($\sim 86 \mu\text{M}$) co-incubated with **1** ($100 \mu\text{M}$) for (D) 0 h and (E) 30 h.

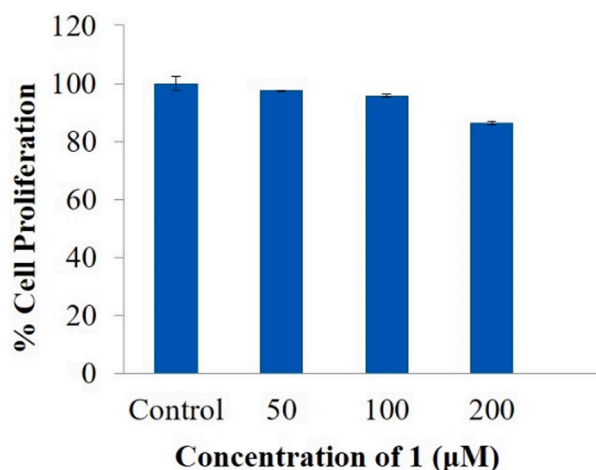


Fig. 7. MTT assay in HeLa cells treated with varied concentrations of compound **1** for 24 h. After 24 h of treatment cell survival values of treated or untreated cells were represented as percentage of cell proliferation.

were later blocked in 1% Bovine serum albumin and stained with FITC-Phalloidin and DAPI solution. The samples were washed with PBS and mounted on glass slides. Further, the cellular morphology was visualized using Confocal Laser Scanning Microscopy (CLSM) using appropriate lasers (Figs. 9 & S8).

2.11. Apoptosis assay

Insulin (~86 µM) with or without compound **1** (100 µM) were first incubated at 65 °C in PBS buffer (pH 7.4) for 48 hrs. HeLa cells in log phase (5×10^4 cells/well) were cultured in 24 well plate at 37 °C in a humidified incubator containing 5% CO₂ (v/v). Subsequently, the cells were treated with incubated human insulin and compound **1** co-incubated human insulin for 24 h. Untreated HeLa cells were taken as negative control in this assay. After 24-hour treatment, the cells were washed thrice with PBS and stained with acridine orange (AO) (100 µg/ml in PBS) and ethidium bromide (EtBr) (100 µg/ml in PBS) at room temperature for 10 min. The stained samples were analysed by confocal microscopy (Fig. 10). Cell apoptosis percentage was quantified as the number of apoptotic cells divided by the total number of cells (Fig. 11). Quantification of cells were carried out by ImageJ software (n = 3).

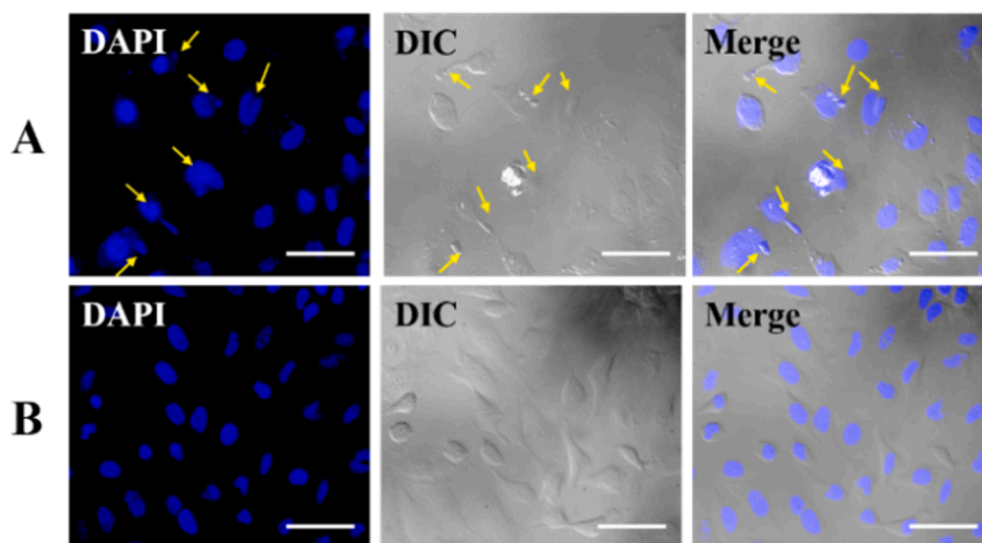


Fig. 8. Morphology of HeLa cells after 24-hour treatment with insulin fibrils stained with Hoechst 33342. Fluorescence microscopy images of (A) Cells treated with 48 h aged insulin (~86 µM) (B) Cells treated with sample of 48 h aged insulin (~86 µM) co-incubated with **1** (100 µM). Nuclear fragmentations were marked with yellow arrows showing fragmented condensed nuclei as well as nuclear blebbing. (Scale bar – 50 µm). (For interpretation of the references to colour in this figure legend, the reader is referred to the web version of this article.)

3. Results and discussion

3.1. Insulin fibrillation kinetics

Thioflavin T (ThT) dye binding was used to study effect of **1** and a control tripeptide Trp-Trp-Tau on insulin aggregation. Amyloidogenic incubation conditions were used in these assays consisting of elevated temperature (65 °C), acidic environment (pH 1.6) and higher salt concentration (25 mM NaCl) [12]. Compound **1** (100 µM) and Trp-Trp-Tau (100 µM) were co-incubated with human insulin (0.5 mg/mL or ~ 86 µM) separately and their effect on aggregation were assessed. Notably, ThT fluorescence was negligible for human insulin throughout the early incubation period in absence or presence of these peptide ligands. Whereas, a sharp exponential rise in ThT fluorescence was observed after a lag phase of 8 h for only insulin. Although Trp-Trp-Tau was able to suppress ThT fluorescence for a shorter duration, but a remarkable anti-amyloidogenic effect was observed for compound **1** with a longer lag phase and significant decrease in ThT fluorescence afterwards (Fig. 2). Native secondary structure stabilization of insulin in presence of **1** was also inferred by both fourier-transform infrared (FTIR) spectroscopy and circular dichroism (CD) spectroscopy.

3.2. Protein conformation analysis

CD spectra pattern of native insulin is characterized by two negative minima around 208 nm and 222 nm reflecting the α-helix rich structure, whereas, insulin fibrils consisting of cross-β sheet like structure can be identified with a negative peak around 218 nm [12]. Transformation of α-helix rich native human insulin towards β-sheet rich fibrillar bodies was observed after 8 h of incubation under amyloidogenic conditions. Notably, co-incubation with compound **1** (100 µM) prevented the loss of the α-helix rich native structure of human insulin (~86 µM) for a significant duration (Fig. 3).

Although this compound was able to maintain α-helix content of human insulin in spite of harsh incubating conditions, there is slight decrease in protein helicity. This can be correlated with the slight increase of ThT fluorescence in the later phase of incubation of insulin in presence of compound **1**. In order to gain knowledge about secondary structure of insulin, signature amide I band pattern of different FTIR spectra have been analyzed (Fig. 4) [9]. Amide I band is associated to the C=O stretching and represents α-helix structure with a peak around ~ 1652 cm⁻¹. While in case of transformed β sheet structure the amide I band appears around ~ 1630 cm⁻¹. Under amyloidogenic condition a peak around ~ 1630 cm⁻¹ can be seen after 8 h of incubation along with

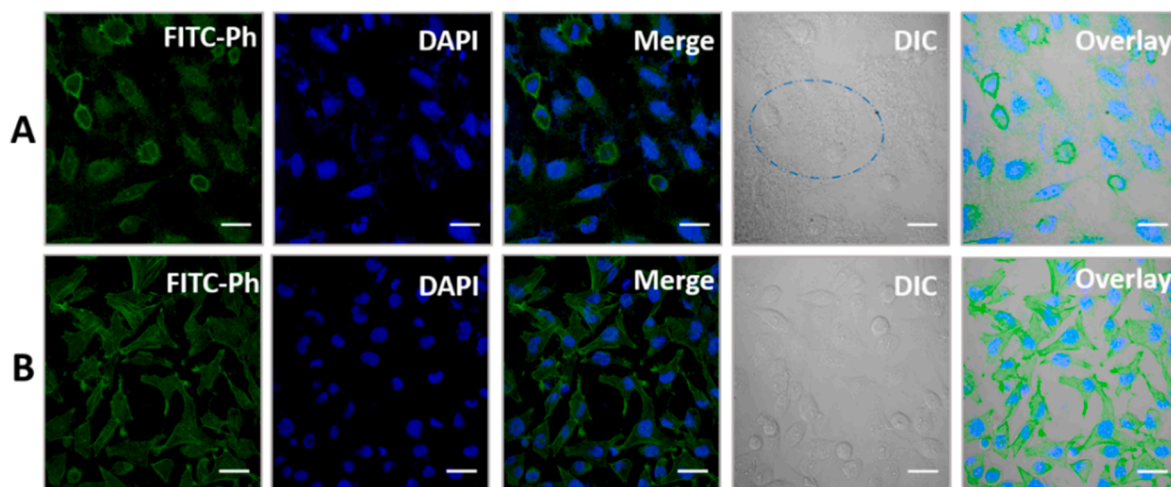


Fig. 9. Confocal laser scanning microscopy images of HeLa cells stained with FITC-phalloidin (Green) and DAPI (Blue) for evaluation of cytoskeletal and nuclear morphology (scale bar – 100 μm). The representative images for (A) HeLa cells treated with 48 h aged human insulin ($\sim 86 \mu\text{M}$) and (B) HeLa cells treated with 48 h aged human insulin ($\sim 86 \mu\text{M}$) co-incubated with **1** (100 μM), both incubated for 24 h. Blue dashed circle in panel A shows the presence of amorphous insulin fibrils around the HeLa cells. (For interpretation of the references to colour in this figure legend, the reader is referred to the web version of this article.)

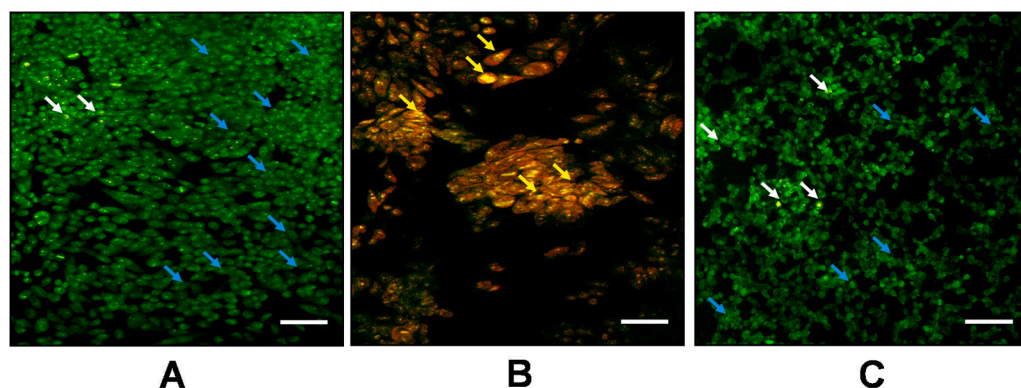


Fig. 10. Detection of apoptosis by AO/EtBr staining in HeLa cells incubated with human insulin and compound **1** for 24 h. The representative images for (A) Untreated HeLa cells, (B) HeLa cells treated with 48 h aged human insulin ($\sim 86 \mu\text{M}$) and (C) HeLa cells treated with 48 h aged human insulin ($\sim 86 \mu\text{M}$) co-incubated with **1** (100 μM). [Blue arrow- viable cells, White arrow- early apoptotic cells, Yellow arrow- late apoptotic cells] (Scale bar: 100 μm). (For interpretation of the references to colour in this figure legend, the reader is referred to the web version of this article.)

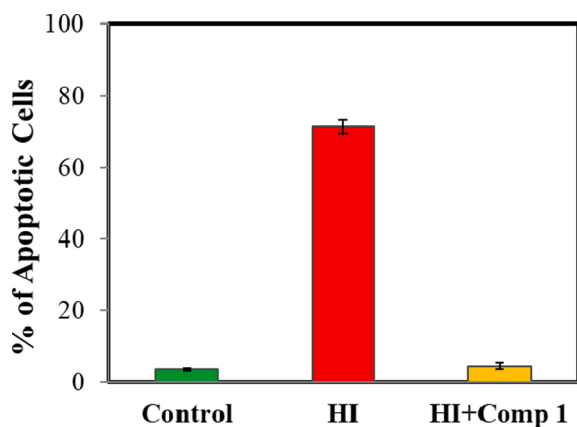


Fig. 11. Quantification of viable and apoptotic cells treated with 48 h aged human insulin ($\sim 86 \mu\text{M}$) and cells treated with 48 h aged human insulin ($\sim 86 \mu\text{M}$) co-incubated with **1** (100 μM). Untreated HeLa cells are taken as control.

the amide I band of α -helix, indicating the transformation of native insulin into cross β sheet rich fibrils. However, insulin ($\sim 86 \mu\text{M}$) co-incubated with compound **1** (100 μM) was able to sustain its amide I band around $\sim 1652 \text{ cm}^{-1}$ signifying sustained helical structure of human insulin for prolonged duration.

Oligomerization status of incubated insulin at different time points were assessed by native polyacrylamide gel electrophoresis (Native PAGE) [29,30]. Initially, dimeric (Molecular weight $\sim 11.6 \text{ kDa}$) form of human insulin in either presence or absence of compound **1** can be observed without any incubation (Fig. 5a & b). Whereas, on heating both monomer (Molecular weight $\sim 5.8 \text{ kDa}$) and dimer (Molecular weight $\sim 11.6 \text{ kDa}$) populations can be seen (Fig. 5c & d). On further heating, in the absence of compound **1** appearance of smear can be observed due to the generation of smaller insulin protofibrils formed during insulin aggregation (Fig. 5e & g). However, for the corresponding time points, insulin co-incubated with compound **1** was able to maintain intact protein bands (Fig. 5f & h). Hence, from this result it can be inferred that in presence of compound **1** human insulin maintains its soluble non-aggregated form even under extreme amyloidogenic conditions.

3.3. Morphological changes using AFM analysis

To visualize the extent of insulin aggregation in absence or presence of this compound, we use atomic force microscopy (AFM) technique [13]. AFM micrographs were collected for samples representing different time points of incubation ranging from 0 to 30 h (Fig. 6). Under amyloidogenic conditions human insulin forms fibrillar bodies of micrometer range even after 10 h of incubation. Significant increase in fibrillar complexity of these insulin aggregates can be observed in AFM as time progresses. But in presence of **1** (100 μM), human insulin (~ 86

μM) exhibits tiny spot like morphologies for a significant duration, representing its non-fibrillar state even in amyloidogenic conditions.

3.4. MTT assay

MTT (3-(4,5-Dimethylthiazol-2-yl)-2,5-Diphenyltetrazolium Bromide) reduction assay was used to analyze cytotoxicity following compound **1** treatment with HeLa cells. Varying concentrations of **1** were added to different sets of cultured HeLa cells in 96-well plate. A set of untreated HeLa cells was used as control. Even after 24 h treatment with different concentrations of compound, overall cell viability was maintained at $\sim 90\%$ compared to control condition (Fig. 7). This study infers the non-cytotoxic nature of compound **1** and opens up further scope to comprehend about its anti-amyloidogenic efficacy in biological conditions.

3.5. Insulin amyloid-mediated apoptotic events and its inhibition

Insulin amyloid mediated cytotoxicity has been reported so far mentioning disruptive inflammatory nature of such fibrils present in injectable insulin dosages. Shielding effect of compound **1** can be appreciated from its maintenance of nearly native secondary structure of insulin for a prolong duration under harsh conditions. Inhibitor assisted reduction in protein aggregate mediated cytotoxicity has already drawn attentions so far [31–34]. Hence, anti-amyloidogenic activity of **1** might also be admired further by screening its potential of reducing insulin fibril mediated cytotoxicity.

Hoechst 33342 dye flawlessly stains condensed DNA of apoptotic cells in greater extent as compared to less condensed nuclei of healthy cells [9]. After treatment with aged insulin ($\sim 86 \mu\text{M}$) co-incubated with compound **1** ($100 \mu\text{M}$) for 24 h, HeLa cells were stained with Hoechst dye to detect changes in nuclei. Apoptotic nuclei seem to present an extremely bright nuclear fluorescence of blue colour (Figure S7A) in case of insulin amyloid treated cells. However, treatment of the cells with compound **1** co-incubated insulin, resulting nuclear fluorescence intensity was less as compared to its earlier counterpart (Figure S7B). Thus, the presence of negligible amount of brighter blue cells affirms protective role of **1** by producing negligible and less toxic insulin amyloids.

Cells treated with insulin fibrils also led to DNA condensation and fragmentation leading to apoptotic membrane protrusions. Cell membrane blebbing and fragmented nuclei are marked with yellow arrows (Fig. 8A). Nuclear condensation and DNA fragmentation lead to polynucleated cells, is also a clear indication of apoptosis [35]. Such polynucleated cells were noticed during the course of treatment of HeLa cells with insulin amyloids (Fig. 9A and S8). However, polynucleated cells were absent in case of HeLa cells treated with compound **1** co-incubated insulin sample due to lack of traceable toxic insulin fibrils (Fig. 9B). Protein aggregates are reported to disrupt native cellular morphology through interactions with cell membrane and generate inflammatory responses in cells leading to sequential apoptotic events in cells [36,37]. FITC-phalloidin and DAPI staining were carried out simultaneously for evaluating cytoskeletal and nuclear integrity respectively of these treated cells. The gross morphology of cytoskeleton and nuclei were visualized using confocal fluorescence microscopy and detected for the cytotoxicity of corresponding insulin samples (Figs. 9 and S8).

Treatment of HeLa cells with insulin fibrils shows disrupted and shortened F-actin, which clearly indicates cell membrane rupturing nature of these toxic fibrils present in background of HeLa cells treated with aged human insulin. Existence of amorphous fibrils around HeLa cells is shown by a blue circle in DIC microscopy image (Fig. 9A). No traceable insulin fibrils were present around HeLa cells treated with compound **1** ($100 \mu\text{M}$) co-incubated insulin ($\sim 86 \mu\text{M}$) (Fig. 9B). Furthermore, it was demonstrated that compound **1** treated insulin did not show any evidence of cytoskeletal disruption.

Furthermore, AO / EtBr dual fluorescent staining was performed to

analyse the morphological changes quantitatively and qualitatively in HeLa cells [38,39]. The two fluorescent probes i.e., AO and EtBr efficiently bind to nucleic acids by intercalation and are utilized to visualize apoptosis and aberrant nuclear changes. Acridine orange is a vital dye which stains green both live and dead cells. Ethidium bromide will stain red only those cells which have lost their membrane integrity. Viable, early apoptotic and late apoptotic cells are stained in green, yellow and orange respectively. Briefly, HeLa cells were treated with aged human insulin and human insulin co-incubated with compound **1** for 24 h and compared with untreated control cells (Fig. 10). In control, uniformly green live cells with normal and intact nucleus were observed (Fig. 10 A). The cells treated with aged human insulin are seen mostly in orange colour and showed significant aberrant morphological changes such as nuclear fragmentation and cell shrinkage indicating late apoptotic stage (Fig. 10 B). Whereas, treatment of cells with compound **1** co-incubated insulin showed presence of viable green cells similar to untreated control cells (Fig. 10 C). However, it is to be noted that a few early apoptotic cells are also observed. These results confirm that compound **1** significantly reduces insulin fibril mediated apoptosis in HeLa cells. Also, cell apoptosis percentage was quantified ($n = 3$) as the number of apoptotic cells divided by the total number of cells (Fig. 11).

Previously we had also done similar studies with different types of conjugates that provide a kind of evidence that Trp-Trp combination is essential to inhibit insulin fibrillation process. However, the conjugate **1** having an additional palmitic acid with Trp-Trp dipeptide and taurine possesses a detergent like property with an intrinsic tendency to self-assemble and in turn plays a pivotal role in insulin amyloidosis inhibition. Given the high value of insulin integrity in injectables, such an approach may lead to a potential breakthrough in insulin amyloid interference and for storage.

4. Conclusions

In conclusion, we have proposed the designing of an inhibitor through fine tuning between its intrinsic polarity and non-polarity in a single platform. Anti-amyloidogenic nature of this compound can also be further acknowledged due to its efficiency in reducing insulin amyloid mediated cytotoxicity. With the advent of its inhibitory as well as cytoprotective role, efficacy of this compound can also be further explored for the chances of being used as anti-aggregating agents in pharmaceutical insulin formulations. Additionally, this compound may also be useful for coating material of insulin injections and storage vials rather than conventionally used silicon oil and teflon coatings reported to promote insulin aggregation.

Author contributions

The manuscript was written through contributions of all authors. All authors have given approval to the final version of the manuscript.

Declaration of Competing Interest

The authors declare that they have no known competing financial interests or personal relationships that could have appeared to influence the work reported in this paper.

Acknowledgements

SV thanks SERB for a J C Bose Fellowship. SG thanks DBT for a Tata Innovation Fellowship. This work is partly supported by SERB project (SG, SV) and DST Nano Mission (SS, SV). S. Sen and P. Singh acknowledge MHRD for pre-doctoral fellowship. NKM thanks CSIR-UGC for a pre-doctoral research fellowship. We thank the Centre for Nanoscience and Soft Nanotechnology and Advanced Centre for Materials Science (ACMS), IIT Kanpur, for access to instrument facilities.

Appendix A. Supplementary data

Supplementary data to this article can be found online at <https://doi.org/10.1016/j.bioorg.2021.104899>.

References

- [1] F. Chiti, C.M. Dobson, Protein misfolding, functional amyloid, and human disease, *Annu. Rev. Biochem.* 75 (1) (2006) 333–366.
- [2] M.R. Nilsson, Insulin amyloid at injection sites of patients with diabetes, *Amyloid* 23 (2016) 139–147.
- [3] S. Okamura, Y. Hayashino, S. Kore-Eda, et al., Localized amyloidosis at the site of repeated insulin injection in a patient with type 2 diabetes, *Diabetes Care* 36 (2013) 2027.
- [4] S.E. Fineberg, T.T. Kawabata, D. Finco-Kent, et al., Immunological responses to exogenous insulin, *Endocr. Rev.* 28 (2007) 625–652.
- [5] A. Lorenzo, B. Razzaboni, G.C. Weir, et al., Pancreatic islet cell toxicity of amylin associated with type-2 diabetes mellitus, *Nature* 368 (1994) 756–760.
- [6] L.-M. Yan, M. Taterek-Nossol, A. Velkova, et al., Design of a mimic of nonamyloidogenic and bioactive human islet amyloid polypeptide (IAPP) as nanomolar affinity inhibitor of IAPP cytotoxic fibrillogenesis, *Proc. Natl. Acad. Sci.* 103 (2006) 2046–2051.
- [7] S. Elmore, Apoptosis: a review of programmed cell death, *Toxicol. Pathol.* 35 (2007) 495–516.
- [8] B. He, N. Lu, Z. Zhou, Cellular and nuclear degradation during apoptosis, *Curr. Opin. Cell Biol.* 21 (2009) 900–912.
- [9] S. Grudzielanek, A. Velkova, A. Shukla, et al., Cytotoxicity of insulin within its self-assembly and amyloidogenic pathways, *J. Mol. Biol.* 370 (2007) 372–384.
- [10] E. Kachooei, A.A. Moosavi-Movahedi, F. Khodaghali, et al., Inhibition study on insulin fibrillation and cytotoxicity by paclitaxel, *J. Biochem.* 155 (2014) 361–373.
- [11] E. Kachooei, A.A. Moosavi-Movahedi, F. Khodaghali, et al., Oligomeric forms of insulin amyloid aggregation disrupt outgrowth and complexity of neuron-like PC12 cells, *PLoS ONE* 7 (2012) e41344.
- [12] N.K. Mishra, R.N.V. Krishna Deepak, R. Sankaramakrishnan, et al., Controlling in vitro insulin amyloidosis with stable peptide conjugates: a combined experimental and computational study, *J. Phys. Chem. B* 119 (2015) 15395–15406.
- [13] N.K. Mishra, K.B. Joshi, S. Verma, Inhibition of human and bovine insulin fibril formation by designed peptide conjugates, *Mol. Pharm.* 10 (2013) 3903–3912.
- [14] Y. Xin, H. Zhang, Q. Hu, et al., Oligotyrosines inhibit amyloid formation of human islet amyloid polypeptide in a tyrosine-number-dependent manner, *ACS Biomater. Sci. Eng.* 5 (2019) 1092–1099.
- [15] J.S. Katz, Y. Tan, K. Kuppannan, et al., Amino-acid-incorporating nonionic surfactants for stabilization of protein pharmaceuticals, *ACS Biomater. Sci. Eng.* 2 (2016) 1093–1096.
- [16] M.I. Ivanova, S.A. Sievers, M.R. Sawaya, et al., Molecular basis for insulin fibril assembly, *Proc. Natl. Acad. Sci. U.S.A.* 106 (2009) 18990–18995.
- [17] A. Rabiee, A. Ebrahim-Habibi, A. Ghasemi, et al., How curcumin affords effective protection against amyloid fibrillation in insulin, *Food Funct.* 4 (2013) 1474–1480.
- [18] S.R. Chowdhury, S. Mondal, P.K. Iyer, Blocking oligomeric insulin amyloid fibrillation via perylenebisimides containing dipeptide tentacles, *ACS Biomater. Sci. Eng.* 4 (2018) 4076–4083.
- [19] H. Skaat, G. Belfort, S. Margel, Synthesis and characterization of fluorinated magnetic core-shell nanoparticles for inhibition of insulin amyloid fibril formation, *Nanotechnology*. 20 (2009) 225106.
- [20] S.-H. Wang, X.-Y. Dong, Y. Sun, Effect of (–)-epigallocatechin-3-gallate on human insulin fibrillation/aggregation kinetics, *Biochem. Eng. J.* 63 (2012) 38–49.
- [21] Y. Hong, L. Meng, S. Chen, et al., Monitoring and inhibition of insulin fibrillation by a small organic fluorogen with aggregation-induced emission characteristics, *J. Am. Chem. Soc.* 134 (2012) 1680–1689.
- [22] L. Nielsen, R. Khurana, A. Coats, et al., Effect of environmental factors on the kinetics of insulin fibril formation: elucidation of the molecular mechanism, *Biochemistry* 40 (2001) 6036–6046.
- [23] V. Sluzky, A.M. Klibanov, R. Langer, Mechanism of insulin aggregation and stabilization in agitated aqueous solutions, *Biotechnol. Bioeng.* 40 (1992) 895–903.
- [24] S.H. Mollmann, J.T. Bukrinsky, S. Frokjaer, et al., Adsorption of human insulin and AspB28 insulin on a PTFE-like surface, *J. Colloid Interface Sci.* 286 (2005) 28–35.
- [25] S. Mauri, M. Volk, S. Byard, et al., Stabilization of insulin by adsorption on a hydrophobic silane self-assembled monolayer, *Langmuir* 31 (2015) 8892–8900.
- [26] G. Carta, E. Murru, S. Banni, et al., Palmitic acid: physiological role, metabolism and nutritional implications, *Front. Physiol.* 8 (2017) 902.
- [27] S. Bag, S. Chaudhury, D. Pramanik, et al., Hydrophobic tail length plays a pivotal role in amyloid beta (25–35) fibril–surfactant interactions, *Proteins* 84 (2016) 1213–1223.
- [28] S.-S. Wang Steven, Kuan-Nan Liu, Tzu-Chiang Han, Amyloid fibrillation and cytotoxicity of insulin are inhibited by the amphiphilic surfactants, *Biochim. Biophys. Acta (BBA) - Molecular Basis of Disease* 1802 (2010) 519–530.
- [29] K. Dubey, B.G. Anand, D.S. Shekhawat, et al., Eugenol prevents amyloid formation of proteins and inhibits amyloid-induced hemolysis, *Sci. Rep.* 7 (2017) 40744.
- [30] A. Velkova, M. Taterek-Nossol, E. Andreetto, et al., Exploiting cross-amyloid interactions to inhibit protein aggregation but not function: nanomolar affinity inhibition of insulin aggregation by an IAPP mimic, *Angew. Chemie - Int. Ed.* 47 (2008) 7114–7118.
- [31] A. Henning-Knechtel, S. Kumar, C. Wallin, et al., Designed cell-penetrating peptide inhibitors of amyloid-beta aggregation and cytotoxicity, *Cell Rep. Phys. Sci.* 1 (2) (2020) 100014.
- [32] S. Mondal, V. Kumar, S.R. Chowdhury, et al., Template-mediated detoxification of low-molecular-weight amyloid oligomers and regulation of their nucleation pathway, *ACS Appl. Bio Mater.* 2 (2019) 5306–5312.
- [33] S. Mondal, S.R. Chowdhury, M. Shah, et al., Nanoparticle assisted regulation of nucleation pathway of amyloid tetramer and inhibition of their fibrillation kinetics, *ACS Appl. Bio Mater.* 2 (2019) 2137–2142.
- [34] S.R. Chowdhury, M. Agarwal, N. Meher, et al., Modulation of amyloid aggregates into nontoxic coaggregates by hydroxyquinoline appended polyfluorene, *ACS Appl. Mater. Interfaces* 8 (2016) 13309–13319.
- [35] K. Janik, C. Treda, A. Włodarczyk, et al., A way to understand idiopathic senescence and apoptosis in primary glioblastoma cells – possible approaches to circumvent these phenomena, *BMC Cancer* 19 (2019) 923.
- [36] E. Takada, K. Okubo, Y. Yano, et al., Molecular mechanism of apoptosis by amyloid β -protein fibrils formed on neuronal cells, *ACS Chem. Neurosci.* 11 (2020) 796–805.
- [37] Z. Du, Y. Guan, C. Ding, et al., Cross-fibrillation of insulin and amyloid β on chiral surfaces: chirality affects aggregation kinetics and cytotoxicity, *Nano Res.* 11 (2018) 4102–4110.
- [38] Kashibhatla, et al., Acridine orange/ethidium bromide (AO/EB) staining to detect apoptosis, *Cold Spring Harb. Protoc.* (2006), <https://doi.org/10.1101/pdb.prot4493>.
- [39] Elumalai, et al., Induction of apoptosis in human breast cancer cells by nimbolide through extrinsic and intrinsic pathway, *Toxicol. Lett.* 215 (2012) 131–142.